DOI 10.5162/iCCC2024/P8

Low-Power Radio-Free Sensor System based on Li-Fi and Optical Wireless Power Transfer

Philipp Meißner[1], René Kirrbach[1], Alexander Noack[1], Tobias Schneider[1], Kai Schmieder[1], Günter Mußbach[2], Frank Wendler[3]
[1] Fraunhofer IPMS, Dresden, Germany,
[2] Bayern-Chemie GmbH, Aschau am Inn, Germany,
[3] MBDA Deutschland GmbH, Schrobenhausen, Germany,
philipp.meissner@ipms.fraunhofer.de

Summary:
This work demonstrates a self-sufficient health and usage monitoring system (HUMS) without any wired or RF-based communication and power transfer. Instead, the wireless, radio-free (WRF) system uses optical wireless communications (OWC) and optical wireless power transfer (OWPT) optimized for a user-friendly operation. The system is capable of live data streaming and long-term data-logging.

Keywords: optical wireless communication, optical wireless power transfer, simultaneous light wave information and power transfer, light-fidelity, condition monitoring, self-sufficient sensor system

Introduction

Recent advancements in microelectronics have facilitated the development of energy-efficient sensor nodes [1]. These nodes can be used in a wide range of applications such as consumer and industrial electronics, defense, and aerospace. A well-suited illustration in the defense sector is condition monitoring for In-Service Surveillance of Munitions [2], where systems can be subjected to significant loads. The storage and operation of military systems require the use of HUMS to ensure high system availability [3]. Wireless connectivity is highly desired, but commonly used radio frequency (RF) signals have limitations in military and munitions applications. A promising alternative method for wireless power and data transmission is a combination of OWC and OWPT, as presented in [4].

Fundamental progress in the field of condition monitoring of solid rocket motors was achieved by Bayern-Chemie [5]. A subsequent collaboration between Fraunhofer IPMS, MBDA and Bayern-Chemie focused on optical communication via Light-Fidelity (Li-Fi) [6]. However, the previous demonstrator did not feature OWPT and relied on an internal battery. In the new demonstrator presented herewith, we investigate the potential of OWC and OWPT for a low-power, self-sufficient WRF HUMS. The WRF approach offers several advantages for military systems in safety-critical environments.

Compared to RF communication, OWC is beneficial regarding safety and security. It is spatially confined, has no RF emissions and has lower sensitivity to electromagnetic interference. OWC, also known as Li-Fi, achieves data rates in the Mbps or even Gbps range [7, 8]. OWPT does not require precise alignment or any physical contact between the transmitter and receiver, making it easy to use. The receiver can also harvest energy from ambient light. By using OWPT and ambient light charging, regular battery changes can be avoided. In some applications, the use of batteries, which are inherently problematic in munitions environments, can be eliminated. Compared to other energy harvesting techniques, such as from kinetic energy [9], OWPT transmits sufficient power up to several watts.

System Concept

The system architecture is shown in Fig. 1. It consists of two separate handheld devices. One is the sensor module and the other one is the reader module. The reader module enables the user to read out sensor data via OWC while powering the sensor module via OWPT at the same time. There are two use cases for the sensor module in terms of data collection. When the reader module is present, a live sensor data stream is established (live stream mode). The second use case covers the absence of the reader module. In this logging mode, all sensor data should be stored in an on-board memory and be transmitted next time the reader module connects. The WRF demonstrator measures temperature, pressure and humidity.

DOI 10.5162/iCCC2024/P8

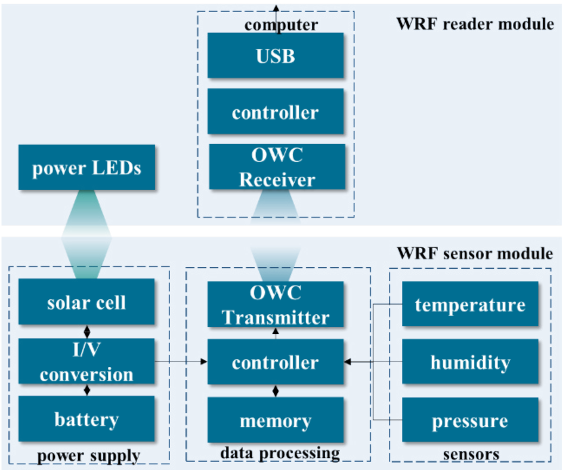

Fig. 1. WRF system architecture

For the logging mode, energy storage is required to power the system when there is insufficient ambient light or between OWPT events. Supercapacitors constitute no viable option due to their high self-discharge rate compared to typical lithium-ion battery cells [10]. To maintain a compact WRF demonstrator, a small battery with very low self-discharge rates, like those found in mobile in-ear headphones, is preferred.

Solar cells (SCs) can be used as OWPT receptors to charge the battery and supply the system with energy. However, due to their low efficiency η_{SC} (typically not much more than 0.15), amorphous and polycrystalline Si-based SCs are not suitable for this system [11, 12]. Monocrystalline Si-SCs, on the other hand, have higher efficiencies of 0.25 or even higher [12] over the solar spectrum. Monocrystalline Si-SCs are the favored option due to their lower cost and higher availability, despite GaAs-SCs outperforming other types with η_{SC} up to 0.5.

To match the monocrystalline SC in terms of light spectrum, we select an OWPT light source in the near-infrared (NIR) spectrum. The data readout should be possible without exact aiming. Therefore, light-emitting diodes (LEDs) appear to be a good choice. In contrast to laser diodes, LEDs are cost-effective and typically eye-safe.

A computer or mobile device can be connected to the reader module to display stored and real-time data.

Measurements and Results

To demonstrate the overall WRF concept and identify a suitable OWPT setup, the work is divided into three parts:

1. *Characterization* of high-power LEDs and SCs to evaluate the OWPT in an initial setup.
2. *Optical simulation* of the final setup to gain an understanding of range and field of view (FOV).
3. *Experimental validation* of the demonstrator in terms of range, FOV and lifetime.

Characterization

The setup for the initial OWPT test is shown in Fig. 2. It features two high-power NIR LEDs and two Si-SCs. The distance is $z_{\mathrm{OWPT}} = 5$ cm. No lenses are used. The SCs have an area of 100 cm² and an efficiency of 0.41 at the LED's wavelength of 940 nm. Both SCs are connected to the charger circuit, which is equipped with a battery.

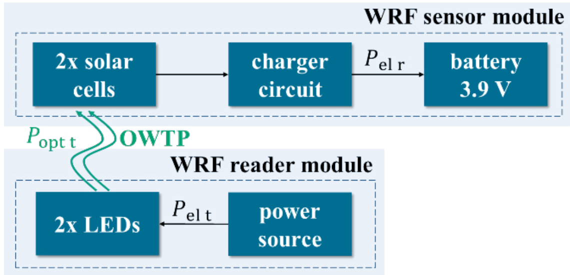

Fig. 2. Initial OWPT characterization setup

The OWPT transmitter achieves a maximum optical power of $P_{\mathrm{opt\,t}} = 2.4$ W, while consuming an electrical power of $P_{\mathrm{el\,t}} = 5$ W. This enables the reader module to be a portable device in the future. The charging circuit of the sensor module feeds $P_{\mathrm{el\,r}} = 140.4$ mW to the battery. According to equation (1) we can calculate an overall transfer efficiency of $\eta_{\mathrm{OWPT}} = 2.81$ %.

$$\eta_{\mathrm{OWPT}} = \frac{P_{\mathrm{el\,r}}}{P_{\mathrm{el\,t}}} = \frac{140.4\,mW}{5\,W} = 2.81\ \% \qquad (1)$$

Optical Simulation

The SCs are a series connection of unit cells. It is mandatory to illuminate the SCs as homogeneously as possible to achieve a high efficiency. Ideally, this homogeneity is also maintained in the optical nearfield, i.e., when the SCs are near the OWPT LEDs. Due to the large SC size, it is very challenging to achieve this homogeneity with one or two LEDs. However, we can solve the issue by using an LED array. With only 3 x 3 LEDs we achieve a good trade-off between array size and complexity. Increasing the LED number enables reducing the power and thermal load per LED and improves lifetime and efficiency.

Although the transfer efficiencies of the initial characterization were promising, the experimental distance was impractical low with only $z_{\mathrm{OWPT}} = 5$ cm. This was necessary due to the

DOI 10.5162/iCCC2024/P8

very broad emission profile of the LEDs. To increase the range, we use a reflector for each LED to direct the light into the FOV.

Fig. 3 (a) shows a raytracing simulation of the incident optical flux Φ_{SC} on the SCs over the distance z_{OWPT} and a lateral displacement x_{OWPT}. Fig. 3 (b) shows the transferred OWPT power P_{OWPT} at the sensor, available to power the sensor module. For the simulation we use an array of 3 x 3 LEDs and a realistic 3D model of the reflector. Each LED has an optical output of Φ_{LED} = 0.26 W (24.1 dBm) that results in a total optical output of 2.34 W (33.7 dBm). For the raytracing simulation, we use realistic ray files and trace 90000 rays for each position. For the simulation of P_{OWPT} we additionally apply a SC fill factor of FF = 0.7, a conversion efficiency of η_{sc} = 0.41 and a charger efficiency of η_{el} = 0.98.

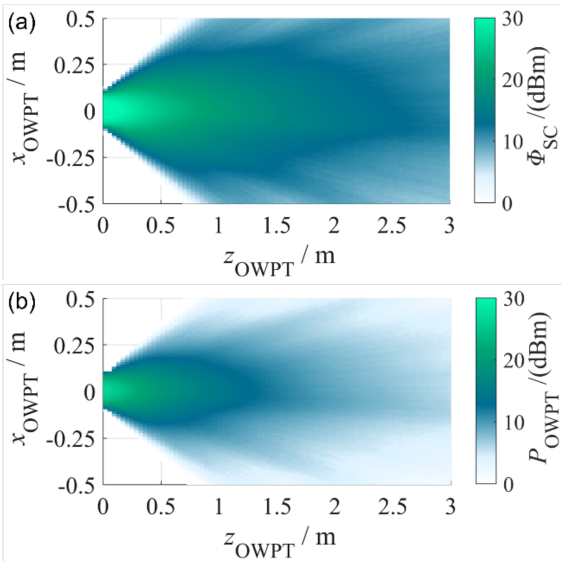

Fig. 3. (a) Incident optical flux Φ_{SC} onto the SCs via OWPT versus alignment. (b) OWPT power P_{OWPT} that is available for powering the sensor module.

There is a large dynamic of the available power depending on the alignment. If we assume that at least $P_{\mathrm{OWPT\,min}}$= 10 dBm is required for the live stream mode, the OWPT is sufficient for distances of up to 175 cm on the optical axis. At z_{OWPT} = 40 cm a lateral displacement of x_{OWPT} = ± 20 cm is tolerable. This corresponds to an FOV full angle θ_{OWPT} = 40°. For distances larger than 0.5 m, θ_{OWPT} is decreasing.

The simulation shows a strong peak of the incident flux with Φ_{SC} = 32.9 dBm (1950 mW). There is still a sufficient safety margin since the SCs can manage a peak power of up to 37.4 dBm (5496 mW). Similarly, our charging circuit can convert up to 35.3 dBm (3400 mW), which is well above the maximum observed OWPT power of P_{OWPT} = 27.3 dBm (537 mW).

Experimental Test

Fig. 4 shows a photograph of the WRF demonstrator. The sensor module has a size of 138 mm x 98 mm x 17 mm and the reader module a size of 139 mm x 101 mm x 39 mm.

Fig. 4. Left: sensor module. Right: reader module.

For the experimental validation, we place the sensor and reader module in front of each other and vary distance z_{OWPT} and lateral alignment x_{OWPT}. Within each point we check if the OWPT delivers sufficient power and if the OWC data transfer is error-free. Fig. 5 shows the results. The OWPT ranges up to $z_{\mathrm{OWPT\,max}}$ = 150 cm, which is slightly lower than in our simulation. At a distance of z_{OWPT} = 40 cm the full angle FOV θ_{OWPT} = 45°, which is slightly larger compared to our simulation, indicating, that the OWPT sender has a slightly broader emission profile compared to the simulation. The OWC range is with $z_{\mathrm{OWC\,max}}$ = 110 cm smaller than the OWPT. At a distance of z_{OWC} = 40 cm the full angle FOV is θ_{OWC} = 32°.

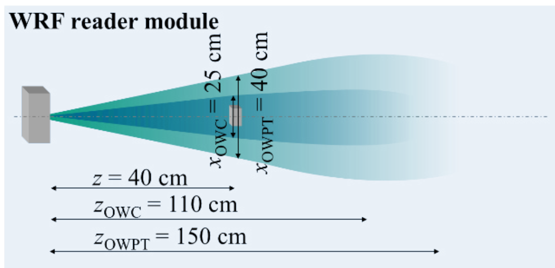

Fig. 5. OWPT and OWC range and alignment of the WRF reader module

The remaining operating time t_{on} of the sensor module after an OWPT event is determined by the energy stored in the battery E_{bat} and the power consumption of the sensor module. Without ambient light, the sensor module is only powered by OWPT events. E_{bat} is calculated according to equation (2).

$$E_{\mathrm{bat}} = (P_{\mathrm{OWPT}} - P_{\mathrm{OWC}}) \cdot t_{\mathrm{OWPT}} \qquad (2)$$

Since the OWC is active whenever the OWPT is active, the power consumed by the OWC, P_{OWC}, is subtracted by the transferred OWPT power P_{OWPT}. The result is multiplicated by the OWPT duration. We assume $t_{\text{OWPT}} = 30$ s. t_{on} is calculated by dividing E_{bat} by the power consumption P_{sensor} according to equation (3).

$$t_{\text{on}} = \frac{E_{\text{bat}}}{P_{\text{sensor}}} = \frac{(P_{\text{OWPT}} - P_{\text{OWC}}) \cdot t_{\text{OWPT}}}{P_{\text{sensor}}} \quad (3)$$

Tab. 1 shows t_{on} depending on the distance z_{OWPT}. Thereby, $t_{\text{on 1}}$ denotes the lifetime of the demonstrator, that features a high power consumption of $P_{\text{sensor 1}}$ = 2.96 mW. As a result, $t_{\text{on 1}}$ is short for all distances. Even for a small distance of 10 cm, $t_{\text{on 1}}$ is only 0.95 h. However, implementing power saving features provides significant potential to reduce the sensor power consumption to $P_{\text{sensor 2}}$ = 20 µW. This would increase the lifetime $t_{\text{on 2}}$ to days or even weeks.

Tab. 1. OWPT single event (30 s) power budget

z_{OWPT}	P_{OWPT}	P_{OWC}	E_{bat}	$t_{\text{on 1}}$	$t_{\text{on 2}}$
cm	mW	mW	J	h	h
4	490	25	14.0	1.31	194.4
10	363	25	10.1	0.95	140.3
20	224	25	6.0	0.56	83.0
40	115	25	2.7	0.25	37.5
100	30	25	0.15	0.01	2.1

Discussion

The WRF demonstrator shows the feasibility of the all-optical WRF sensor concept. The geometric dimensions of the sensor module would allow the WRF demonstrator to be used for realistic applications during In-Service Surveillance of munitions. A full-angle 32° FOV for the OWC allows for practical usability. The slightly larger OWPT FOV compared to the OWC FOV ensures that the OWC will always have sufficient power, once the OWC channel is adequately aligned.

The power budget is sufficient for live sensor data steaming. However, the remaining operating time from a single OWPT event is rather short for the present WRF demonstrator. The current solution requires multiple OWPT events at short intervals, which could be achieved primarily in automated environments. The demonstrator can be powered by ambient light if the harvested power is ≈ 3 mW. This would require an irradiance of E_{amb} = 1.2 W/m². The most promising approach, therefore, is the reduction of the power consumption of the sensor device, as the values of $t_{\text{on 2}}$ in Tab. 1 indicate. The demonstrator has potential for improvement by using power saving and power down modes as well as smart data processing.

Summary and Outlook

In this work, we demonstrate an all-optical, wireless, radio-free sensor system. The WRF approach combines OWC and OWPT for condition monitoring. The developed HUMS consists of a sensor module and a reader module. It provides live data streaming with a range of more than 1 m and a user-friendly FOV with 32° full angle. In addition, the sensor module can record data autonomously over time if there is sufficient ambient light or OWPT available. Future work should focus on reduced power consumption of the sensor module to increase the active lifetime. Another future objective could be the miniaturization of both modules.

Acknowledgement

The research work was initiated and funded by MBDA and Bayern-Chemie. We would like to thank both companies for the long-standing, very successful cooperation in the development of innovative Li-Fi solutions for condition monitoring.

References

[1] S. Sudevalayam and P. Kulkarni, "Energy Harvesting Sensor Nodes: Survey and Implications," *IEEE Commun. Surv. Tutorials*, vol. 13, no. 3, pp. 443–461, 2011, doi: 10.1109/SURV.2011.060710.00094.

[2] *NATO Standardization Agreement (STANAG) 4675: "In-Service Surveillance (ISS) of Munitions",* North Atlantic Treaty Organization (NATO), 2017.

[3] *NATO Standardization Agreement (STANAG) 4844: "NATO Handbook for Munitions Health Management",* North Atlantic Treaty Organization (NATO), 2021.

[4] P. D. Diamantoulakis, G. K. Karagiannidis, and Z. Ding, "Simultaneous Lightwave Information and Power Transfer (SLIPT)," *IEEE Trans. on Green Commun. Netw.*, vol. 2, no. 3, pp. 764–773, 2018, doi: 10.1109/TGCN.2018.2818325.

[5] G. Tussiwand, D. Oley, H. Besser, F. P. Weterings, and G. Brouwer, "Application of Embedded Sensors Technology to a Full-Scale Nozzleless Rocket Motor," in *43rd AIAA/ASME/SAE/ASEE Joint Propulsion Conference & Exhibit*, Reston, Virigina, 2007.

[6] NATO Science and Technology Organization (STO), "AVT-292-CDT Cooperative Demonstration of Technology on Munition Health Management Final Report," in *STO-TR-AVT-292, 2021*.

[7] R. Kirrbach, M. Faulwaßer, B. Jakob, T. Schneider, and A. Noack, "Li-Fi for Augmented Reality Glasses: A Proof of Concept," in *2019 IEEE International Symposium on Mixed and Augmented Reality Adjunct (ISMAR-Adjunct)*, Beijing, China, 102019, pp. 263–268.

[8] R. Kirrbach, M. Faulwaßer, M. Stephan, T. Schneider, and F. Deicke, "High Power Eye-Safe Optical Wireless Gigabit Link Employing a Freeform Multipath Lens," *IEEE Commun. Lett.*, vol. 26, no. 6, pp. 1343–1347, 2022, doi: 10.1109/LCOMM.2022.3162642.

[9] M. Mösch, G. Fischerauer, and D. Hoffmann, "A Self-adaptive and Self-Sufficient Energy Harvesting System," *Sensors (Basel, Switzerland)*, vol. 20, no. 9, 2020, doi: 10.3390/s20092519.

[10] P. Kurzweil and M. Shamonin, "State-of-Charge Monitoring by Impedance Spectroscopy during Long-Term Self-Discharge of Supercapacitors and Lithium-Ion Batteries," *Batteries*, vol. 4, no. 3, p. 35, 2018, doi: 10.3390/batteries4030035.

[11] T. Miyamoto, "Optical wireless power transmission using VCSELs," *Proceddings of SPIE*, vol. 1068204, 2018, doi: 10.1117/12.2309436.

[12] M. Perales *et al.,* "Characterization of high performance silicon-based VMJ PV cells for laser power transmission applications," in *High-Power Diode Laser Technology and Applications XIV*, San Francisco, California, United States, 2016, 97330U.